THE JOURNAL OF PHYSICAL CHEMISTRY C

Article

Cite This: J. Phys. Chem. C 2019, 123, 1645−1652

pubs.acs.org/JPCC

Geometric and Magnetic Structures of K_2ReI_6 as an Antiferromagnetic Insulator with Ferromagnetic Spin-Canting Originated from Spin−Orbit Coupling

Xin Gui,[†] Stuart Calder,[‡] Huibo Cao,[‡] Tianyi Yu,[†] and Weiwei Xie*[,†]

[†]Department of Chemistry, Louisiana State University, Baton Rouge, Louisiana 70803, United States

[‡]Neutron Scattering Division, Oak Ridge National Laboratory, Oak Ridge, Tennessee 37831, United States

Supporting Information

ABSTRACT: We present the results of a crystallographic analysis, magnetic characterization including neutron powder diffraction, and theoretical assessment of K_2ReI_6 prepared using solvent reactions. K_2ReI_6 crystallizes in the space group $P2_1/n$ with an inversion center. Magnetic measurements of K_2ReI_6 sample indicate dominant antiferromagnetic coupling with a Curie−Weiss temperature of $\theta_W = -63.3(1)$ K, effective magnetic moment ~2.64 μ_B/Re but show a weak ferromagnetism ordered at ~24 K. Neutron powder diffraction indicates long-range order of the Re spins below 24 K, with an ordered magnetic moment of 2.2(1) μ_B/Re at 1.5 K. Therefore, a canted antiferromagnetic structure is concluded. The electronic structures using first-principles calculations suggest that the antiferromagnetic model of K_2ReI_6 yields the lowest total energy and opens a band gap with ~1.0 eV width, which is consistent with the UV−vis−NIR optical measurements. After including the spin−orbit coupling (SOC) into the calculation, the band degeneracies slightly shift without influencing the band gap. The results imply that K_2ReI_6 is an antiferromagnetic insulator with weak ferromagnetic spin-canting resulting from strong SOC-entangled ground state $S = 3/2$.

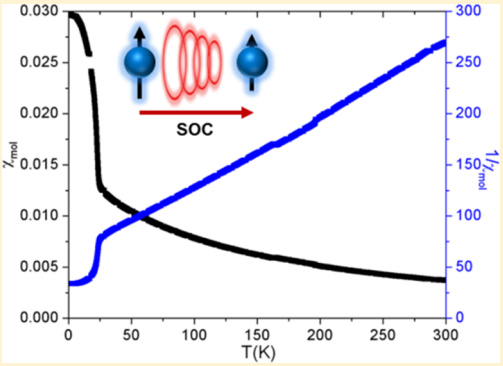

INTRODUCTION

Recently, the importance of spin−orbit coupling (SOC) to generate the electronic ground state in 4d/5d-based compounds has emerged and many novel routes to host unconventional physical states have been revealed, for example, quantum spin liquids,[1−9] Weyl semimetals,[10−12] and axion insulators.[13−15] Such quantum materials with strong SOC may have applications in data storage and memory, electronics, and quantum computing.[16−20] The major experimental and theoretical efforts in quantum spin-liquid state study have been solely undertaken to search for novel spin−orbit coupling systems in various d^5 systems with $S = 1/2$, for example, α-$RuCl_3$.[5,21−27] Few references have been reported concerning other situations, for example, $S = 3/2$, because octahedral d^3 configurations are expected to be orbitally quenched $S = 3/2$ states, in which case SOC enters only as a 3rd-order perturbation.[28−30] Despite this, there is significant experimental evidence that SOC influences the magnetic properties of $5d^3$ transition-metal oxides.[24,31−33] A common magnetic phenomenon related to SOC is spin-canting, which has been widely observed and investigated in many different systems.[34−36] Spin-canting means spins are tilted a small angle about their axis rather than being accurately parallel. Generally, the spin-canting can be attributed to two different sources. The first one is due to the antisymmetric superexchange interaction (the Dzyaloshinskii−Moriya interaction, DMI).[37,38] The other one is the presence of single-ion anisotropy, which provides different preferential directions for the magnetic moments of two types of ions locating on different sublattices. Both DM and anisotropy rely on SOC. Thus, the spin-canting can be considered as a strong hint of large SOC in the different systems.

K_2ReI_6 was initially experimentally synthesized and characterized by both structural and magnetic properties.[39,40] The correct crystal structure of K_2ReI_6, however, remains unresolved possibly due to the crystalline sample quality. One consistent observation, which can be confirmed according to the references, is the shortest Re−Re distance around 7.5−8 Å between two isolated Re@I_6 octahedral clusters. The previous magnetic measurements showed the antiferromagnetic ordering accompanying a weak ferromagnetic moment with a 1.2° canting angle in K_2ReI_6.[39]

Herein, we reported a thorough structural characterization and investigation of the magnetic properties and theoretical electronic structures of K_2ReI_6, in which Re^{4+} adopts a $5d^3$ electronic configuration. We focus on the magnetic ordering in K_2ReI_6 by clarifying the intrinsic interplay of electronic, spin, and orbital degrees of freedom arising from a complex balance

Received: November 24, 2018
Revised: December 29, 2018
Published: January 3, 2019

DOI: 10.1021/acs.jpcc.8b11371
J. Phys. Chem. C 2019, 123, 1645−1652

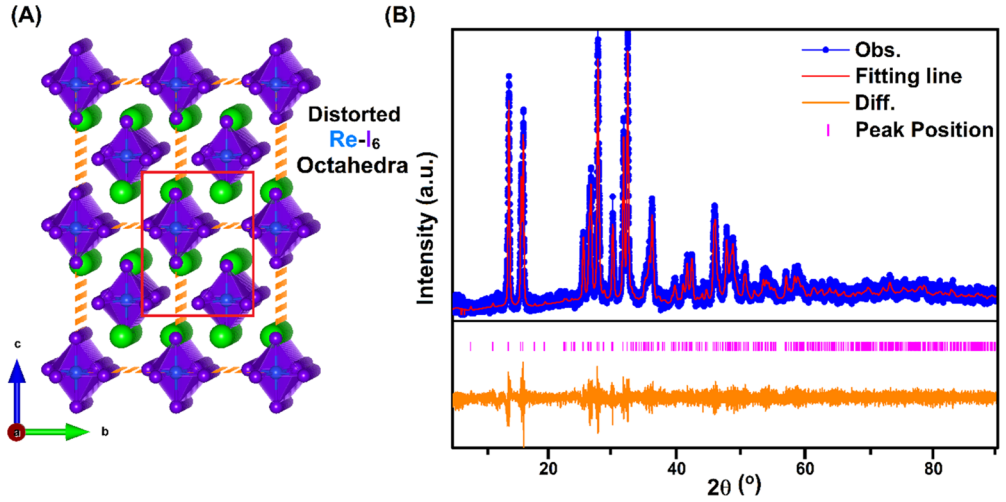

Figure 1. (A) Crystal structure of K_2ReI_6 (green: K atoms; blue: Re atoms; purple: I atoms). The red line indicates the unit cell of reported K_2ReI_6. (B) Powder X-ray diffraction pattern of K_2ReI_6 fitted using the Le-Bail model. The blue line with circle stands for observed pattern. The red line, orange line, and pink tick represent fitted pattern, different between observed and fitted pattern and peak position of K_2ReI_6, respectively.

of electron−electron correlations (U), spin−orbit coupling (SOC), and crystal-field theory in K_2ReI_6. With a combined experimental and theoretical study, we show that K_2ReI_6 is an antiferromagnetic insulator.

METHODS

Sample Preparation of K_2ReI_6. The procedure for sample preparation of K_2ReI_6 is following the previously reported one.[39] $KReO_4$ (≥99%, Alfa Aesar) with amount of 2.0 g (6.8 mmol) was mixed with 6.0 g of KI (36.0 mmol) and were dissolved in 60 mL of 47% HI solution in a 250 mL round-bottom flask. After stirring at 70 °C for 1 h, the dark violet solution was put into a lab use freezer with a temperature of 2 °C for another 0.5 h. The K_2ReI_6 will slowly precipitate and crystallize on the bottom of the flask. The resulting solution with precipitation was vacuum-filtered, and the obtained small crystals were dried at 70 °C in oven overnight. The mass of the dry product is 5.0 g, which leads to a yield of 71.7%.

Phase Identification. We use a Rigaku MiniFlex 600 powder X-ray diffractometer equipped with Cu Kα radiation (λ = 1.5406 Å, Ge monochromator) to determine the phase purity. The Bragg angle was ranging from 5 to 90° in a step of 0.005° at a rate of 0.8°/min. The powder X-ray diffraction (PXRD) pattern was fitted by using Le-Bail model in JANA2006[41] with the calculated pattern generated from the single-crystal X-ray data.

Structure Determination. Crystals from each reaction sample were mounted on the tips of Kapton fibers. Low-temperature intensity data were collected on a Bruker Smart Apex II diffractometer using Mo Kα radiation (λ = 0.71073 Å). Data were collected over a full sphere of reciprocal space by taking seven sets of data with 0.5° scans in ω with an exposure time of 15 s per frame. The 2θ range extended from 6 to 66°. The SMART software was used for data acquisition.[42] Intensities were extracted and corrected for Lorentz and polarization effects using the SAINT program. Empirical absorption corrections were accomplished with SADABS, which is based on modeling transmission by spherical harmonics employing equivalent reflections with $I > 3\sigma(I)$. With the SHELXTL package, the crystal structures were solved using direct methods and refined by full-matrix least-squares on F^2.[43]

Neutron Powder Diffraction (NPD). The magnetic structure was determined by neutron powder diffraction (NPD) performed at HB-2A, Oak Ridge National Laboratory. A Ge (113) monochromator provides a principal wavelength of 2.41 Å. The experiment was carried out at 1.5 and 40 K, respectively, on a ∼1 cm long, ∼6 mm diameter pressed pellet of ∼5 g K_2ReI_6 loaded in an aluminum sample holder. Data were collected from 5 to 127° (2θ) with steps of 0.05° and total counting time of 8 h per temperature. The magnetic structure was obtained by refining neutron data with the Fullprof Suite and SARAh.[44−46] The propagation vector of k = (0,0,0) was determined, and the resulting two different symmetry allowed irreducible representations Γ1 and Γ3 were tested to refine the NPD data. The magnetic scattering generated from Γ1 structure was determined to be the best fit to the pattern.

Magnetization Measurements. The magnetization measurements were performed using a Physical Property Measurement System (PPMS) Dynacool with vibrating sample magnetometer manufactured by Quantum Design, Inc. on K_2ReI_6 crystals. The PPMS operates over a temperature range of 1.8−300 K and in applied fields of up to 90 kOe. NPD at low temperatures also gives magnetic contribution to nuclear Bragg reflections, which facilitates refinement of magnetic moments on each atom.

Electronic Structure Calculations. On the basis of the experimental geometric and magnetic structures of K_2ReI_6, the electronic structure was calculated using WIEN2k with spin−orbit coupling (SOC) included. Spin-polarization using LDA + U (U = 2 eV) was employed in the solely ferromagnetic and antiferromagnetic models investigated. The energy cutoff was 500 eV. Reciprocal space integrations were completed over the 14 × 7 × 7 Monkhorst−Pack k-points mesh with the linear tetrahedron method. With these settings, the calculated total energy converged to less than 0.1 meV per atom.

RESULTS AND DISCUSSION

Crystal Structure of K_2ReI_6 with Inversion Center. We successfully synthesized polycrystalline samples of K_2ReI_6 from

DOI: 10.1021/acs.jpcc.8b11371
J. Phys. Chem. C 2019, 123, 1645−1652

the solvent reaction. The single-crystal X-ray diffraction results are examined carefully and shown in Figure 1A. K_2ReI_6 adopts a monoclinic structure with space group $P2_1/n$ (No. 14) and an inversion center, which is different from the previously reported one, *Pn* (S.G. 7).[39] The red line in Figure 1A encloses the unit cell obtained by previous researchers, whereas the orange dash line is the unit cell we obtained. The volume parameter we obtained (703.8(5) Å^3) is ∼0.9% larger than the reported one (697.45(5) Å^3) with elongation of all three lattice parameters: *a* (7.844(3) vs 7.815(1) Å), *b* (7.896(3) vs 7.874(1) Å), and *c* (11.363(5) vs 11.335(1) Å). Re^{4+} ions occupy the inversion center surrounded by six I^- ions and form octahedral cluster. The $Re@I_6$ octahedron is very slightly distorted with four long Re−I bond interactions (2.729(1) Å) and two short ones (2.726(1) Å). The antiferromagnetic coupling between isolated $Re@I_6$ clusters can be mediated through K^+ ions or Re−I−I−Re superexchange. The $Re@I_6$ octahedron also tilts 8.73(3)° off *c*-axis resulting the monoclinic structure instead of tetragonal K_2PtCl_6-type. Moreover, the titling of $Re@I_6$ clusters could lead to the weak ferromagnetism due to spin-canting, which originates from the existences of antisymmetric interaction and anisotropy. The relatively long distances between the Re ions (7.844(3) to 7.936(3) Å) indicate no direct interactions between Re^{4+} and Re^{4+}. The crystallographic data including atomic positions, site occupancies, and isotropic thermal displacements are summarized in Tables 1 and 2. Anisotropic displacement parameters are shown in Table S1 in the Supporting Information. The phase purity of K_2ReI_6 was examined by powder X-ray diffraction shown in Figure 1B. A high-purity phase of K_2ReI_6 can be indexed, and no additional Bragg peaks can be found according to the PXRD pattern, which means that no impurity can be detected using powder X-ray diffraction.

Table 1. Single-Crystal Refinement for K_2ReI_6 at 299(2) K

refined formula	K_2ReI_6
F.W. (g/mol)	256.45
space group; *Z*	$P2_1/n$; 8
a (Å)	7.844(3)
b (Å)	7.896(3)
c (Å)	11.363(5)
β (°)	90.350(9)
V (Å^3)	703.8(5)
extinction coefficient	0.0067(3)
θ range (°)	3.142−33.152
no. reflections; R_{int}	6586; 0.0363
no. independent reflections	2630
no. parameters	44
R_1: ωR_2 ($I > 2\delta(I)$)	0.0314; 0.0677
goodness of fit	1.047
diffraction peak and hole (e^-/Å^3)	1.486; −1.017

Direct Current Magnetic Susceptibility of Polycrystalline K_2ReI_6. The previous study showed the antiferromagnetic transition in K_2ReI_6 around 24 K. We performed the magnetic properties of polycrystalline sample measured at 500 Oe focusing on the temperature range from 1.8 to 50 K shown in Figure 2. With temperature decreasing from 50 K, the zero-field cooling χ_{mol} marked in blue starts increasing at 24 K to a broad maximum at around 20 K, then drops dramatically to another flat stage at around 15 K. With field cooling, χ_{mol} only shows the transition around 24 K. The transition with zero-field cooling around 20 K may be caused by spin-canting.[47]

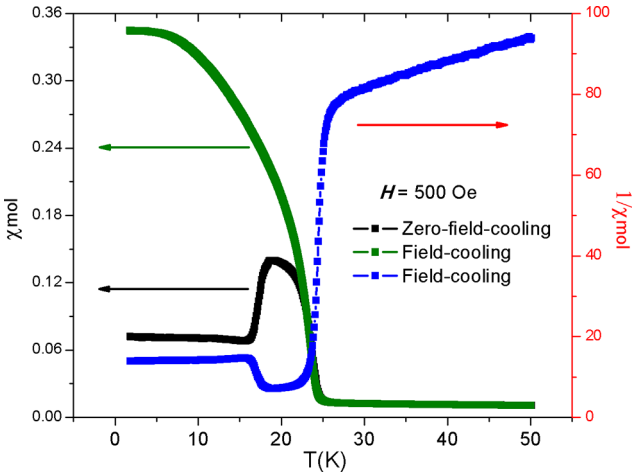

Figure 2. Temperature-dependent magnetic susceptibility of K_2ReI_6 measured at 500 Oe applied field (blue: χ_{mol} with zero-field cooling; green: χ_{mol} with field cooling; red: $1/\chi_{mol}$).

To obtain more information about the magnetic susceptibility, the magnetization $M(T)$ at various applied fields is examined carefully in comparison to $M(H)$ in the temperature range from 18 to 30 K shown in Supporting Information. The magnetizations were measured with the zero-field cooling procedure at 10 kOe illustrated in Figure 3. Different from the magnetic susceptibility measured at 500 Oe, when the applied field increases, the weak ferromagnetism region becomes wider. The magnetization measured at 10 kOe shows that the high applied field removes the antiferromagnetic interactions completely, and only the weak ferromagnetism is kept. Fitting $1/\chi_{mol}$ data above 30 K using the Curie−Weiss law yields an effective moment 2.64 μ_B/Re and a negative $\theta = -63.3(1)$ K, which indicates antiferromagnetic coupling in K_2ReI_6.

L−S Coupling in K_2ReI_6. In heavy atoms, the spin−orbit coupling between the spin and orbital angular momenta cannot be ignored. In K_2ReI_6, Re^{4+} has electron configuration $5d^3$ with a complicated interplay of crystal field and SOC effects

Table 2. Atomic Coordinates and Equivalent Isotropic Displacement Parameters of K_2ReI_6 System[a]

atom	Wyck.	occ.	*x*	*y*	*z*	U_{eq}
Re1	2a	1	0	0	0	0.0253(1)
I2	4e	1	0.1992(1)	0.2811(1)	0.9789(0)	0.0407(1)
I3	4e	1	0.2801(1)	0.7993(1)	0.9721(0)	0.0396(1)
I4	4e	1	0.0527(1)	0.9980(1)	0.2376(0)	0.0457(1)
K5	4e	1	0.9845(3)	0.4550(3)	0.2511(2)	0.0663(5)

[a] U_{eq} is defined as one-third of the trace of the orthogonalized U_{ij} tensor (Å^2).

DOI: 10.1021/acs.jpcc.8b11371
J. Phys. Chem. C 2019, 123, 1645−1652

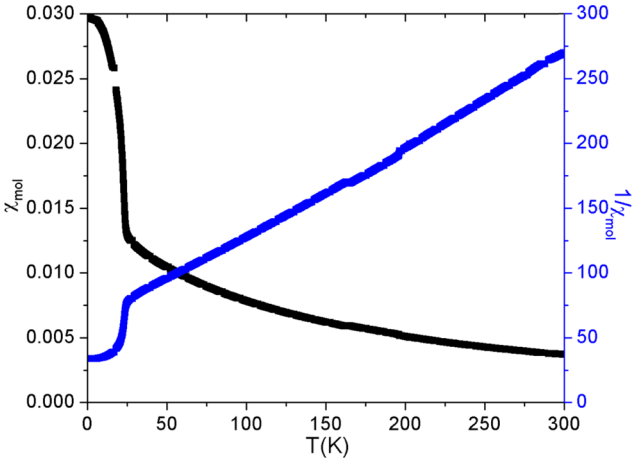

Figure 3. Temperature-dependent magnetic susceptibility and inverse magnetic susceptibility of K_2ReI_6 at 10 kOe applied fields.

illustrated in Figure 4. The effective moment (μ_{eff}) on Re^{4+} (2.64 μ_B) obtained from magnetic susceptibility is much

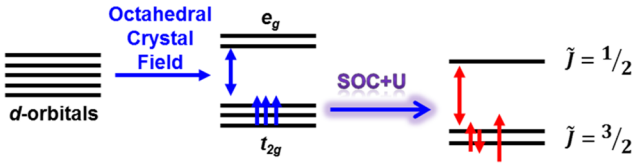

Figure 4. Scheme of $S = 3/2$ in K_2ReI_6 with a d^3 electronic configuration on Re^{4+}.

smaller than the expected spin-only moment result ($\mu_{eff} = \sqrt{n(n+2)}\ \mu_B = \sqrt{15}\ \mu_B = 3.87\ \mu_B$).[48] In K_2ReI_6 with distorted octahedral Re@I_6, the three unpaired electron on Re^{4+} gives the largest value of total spin angular momentum, $S = 3/2$.[49] The expected ordered magnetic moment on Re^{4+} is larger than our experimental measurements from neutron scattering of 2.2(1) μ_B. This also indicates the significant effects from the extended orbitals, for example, covalency, on the magnetic properties of Re^{4+} in K_2ReI_6. To incorporate the SOC into the consideration, the theoretical magnetic moment of Re^{4+} can be obtained through the equation, $\mu = g_J\sqrt{J(J+1)}\ \mu_B$, where g_J is the modified Landé g factor, $g_J = 1 + \frac{J(J+1)+S(S+1)-L(L+1)}{2J(J+1)}$.[50] Accordingly, it is found that $L_p = 0$, $S = 3/2$, and $J = 3/2$ for the system without SOC. As increasing the SOC in the system, the magnetic moments will decrease.

Due to the large Re^{4+}–Re^{4+} distance and weak Re^{4+}–Re^{4+} interactions, we can treat Re^{4+} as a single ion in octahedral coordination. To analyze the temperature-dependent effective magnetic moment on Re^{4+}, the Kotani plot is shown in Figure 5 with p_{eff} ($p_{eff} = \sqrt{8(\chi-\chi_0)T}$) vs kT/λ, where k is the Boltzmann constant, T is the temperature, λ is the system-dependent SOC constant, and $\lambda = 1350\ cm^{-1}$ is used for Re^{4+} in K_2ReI_6.[51] This analysis was first proposed by Kotani, later modified and widely employed for the molecular systems with 4d/5d transition metals by McQueen.[52−54] The ground state in d^3 case is expected to be quartet, and d^3 has no orbital degeneracy according to Kotani's prediction, which means that the orbital motion of electrons has no contribution to the

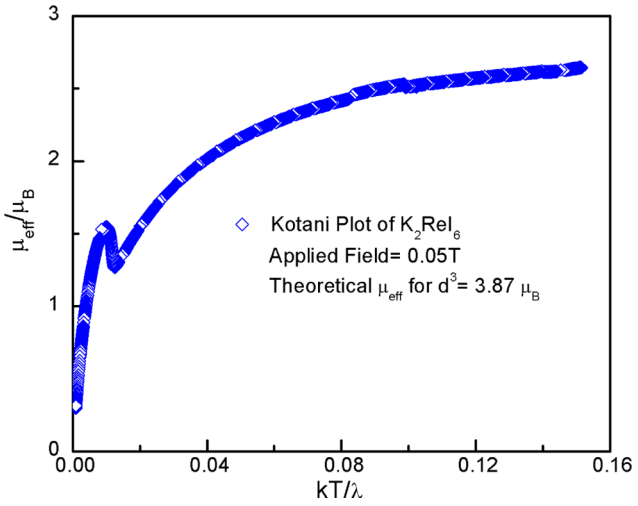

Figure 5. Kotani curve on strongly spin−orbit-coupled K_2ReI_6. The effective magnetic moment p_{eff} per mole of Re^{4+} is calculated by $p_{eff} = \sqrt{8(\chi-\chi_0)T}$.

magnetic moment. The octahedral d^3 configurations are expected to be orbitally quenched, and the μ_{eff} is supposed to be a constant spin-only value 3.87 μ_B. The data for K_2ReI_6 do not follow the expected theoretical results given by the Kotani. This reduction in magnetic moment on d^3 has been observed in several 5d compounds as being due to the extended 5d orbitals leading to a large degree of covalency.[24]

Field-Dependent Magnetization in K_2ReI_6. The field dependences of the magnetization $M(H)$ measured with applied fields up to 90 kOe at 1.8 K is shown in Figure 6. The magnetization increases quickly from zero to ca. 0.022 μB at 500 Oe, later it increases linearly to 0.19 μB till 90 kOe, which is far from the expected saturation value. This also indicates the strong antiferromagnetic interactions between the Re^{4+} ions. The extrapolation to the zero field of the data at high fields (>10 kOe) has a positive intercept (0.023 μB) to the magnetization axis, indicating a weak ferromagnetic behavior. The hysteresis loop at the zero applied field was observed with the coercivity at ∼3.65 kOe. This kind of field-dependent behavior reflects a magnetic transition from an antiferromagnetic state in the form of a spin-canting to a weak ferromagnetic state. To obtain more information of the magnetic phase transitions, the field dependences of $M(H)$ at 150 K were investigated carefully upon both sweeping up and down of the applied field, which shows the paramagnetic properties above the transition temperature.

Magnetic Structure of K_2ReI_6 Determined by Neutron Powder Diffraction. To further understand the exact magnetic structure and magnetic interactions, neutron powder diffraction was carried out on K_2ReI_6 pellet, and the results were refined with the Rietveld method by the Fullprof suite, as shown in Figure 7A. The k-vector was determined to be (0 0 0), which indicates that the antimagnetic unit cell is identical with the crystallographic unit cell. This was utilized in a representational analysis approach to generate irreducible representations (IRs) and basis vectors. Two IRs are symmetry allowed based on the propagation vector and with the Re ion at the (x, y, z) position. Both were refined to arrive at the final result. Two observable magnetic peaks emerge at 12.4 and 17.6°, corresponding to the (001) and (010) reflections. According to the refinement, the magnetic moment is aligned

DOI: 10.1021/acs.jpcc.8b11371
J. Phys. Chem. C 2019, 123, 1645−1652

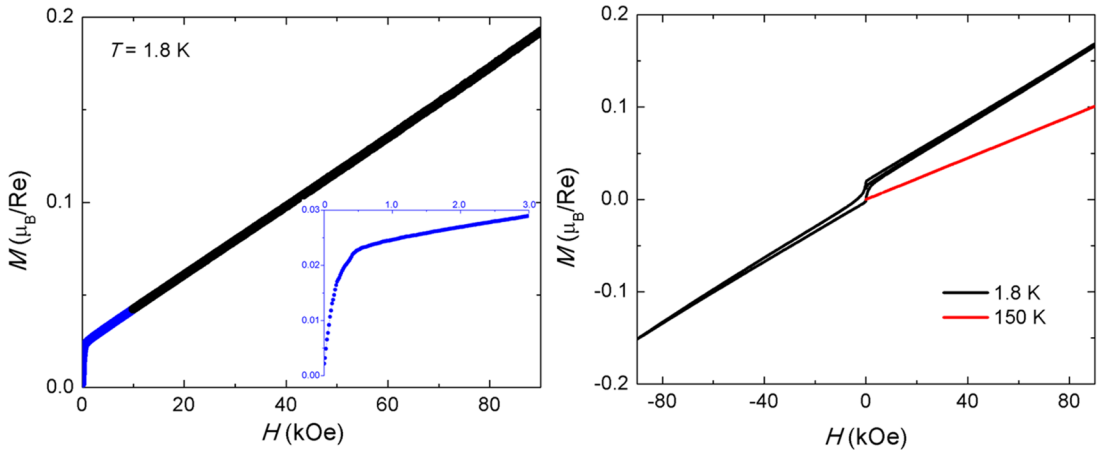

Figure 6. (Left) Field-dependent magnetization of K_2ReI_6 measured at 1.8 K with applied field ranging from 0 to 9 T. (Right) Hysteresis measurements at 1.8 and 150 K from −9 to 9 T.

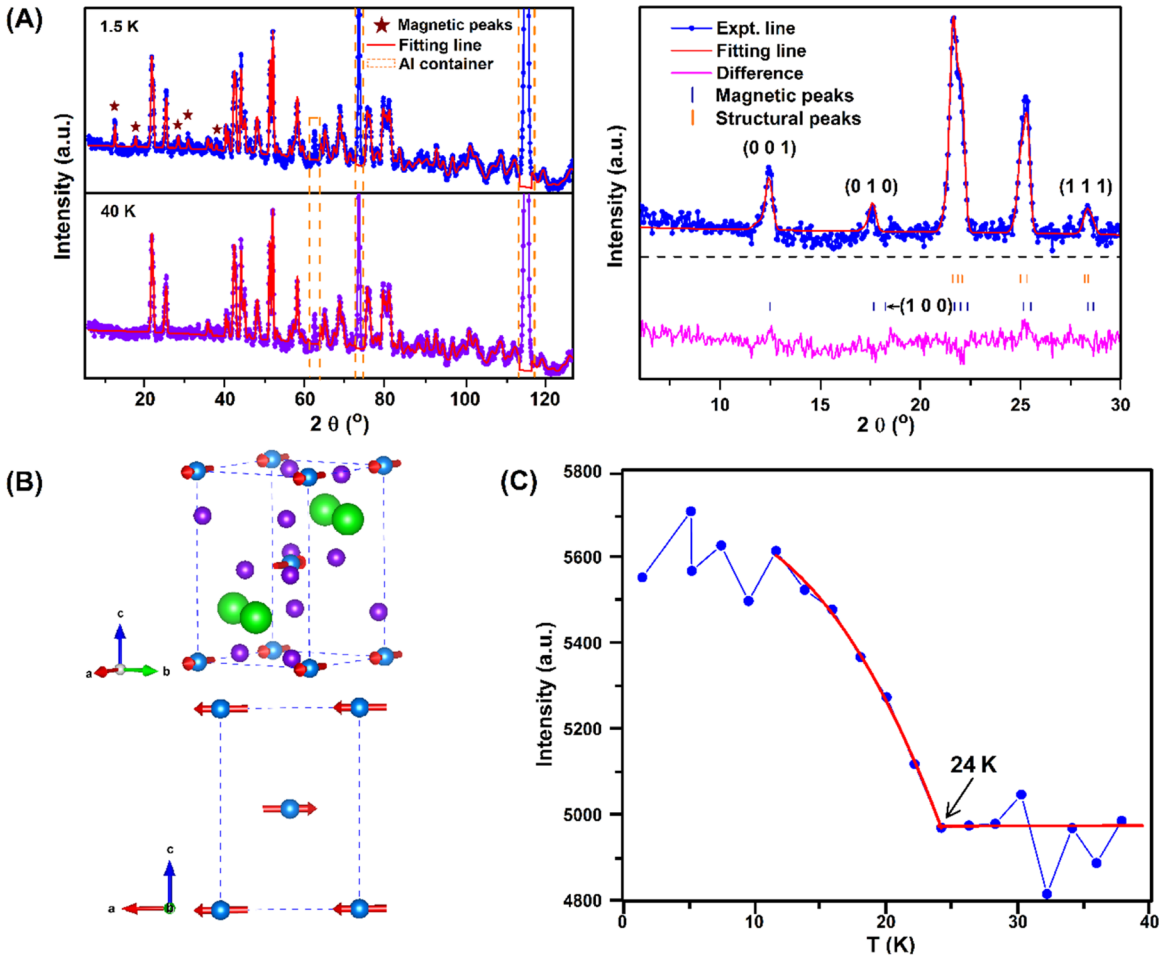

Figure 7. (A) (Left) Rietveld fitting of neutron powder diffraction patterns at 1.5 and 40 K for K_2ReI_6. (Right) Rietveld fitting of NPD pattern at 1.5 K. The blue solid circles, red and pink lines represent observed pattern, fitting line, and difference between experimental and fitting results. Orange and dark blue vertical ticks represent crystal structure and magnetic structure peak positions, respectively. (B) Refined magnetic structure of K_2ReI_6 with magnetic moment. (C) The intensity of the magnetic peak as the temperature changing from 1.5 to 40 K.

with the *a*-axis. Therefore, we determine that the magnetic ground state of K_2ReI_6 is antiferromagnetic (AFM), which is illustrated in Figure 7B, with the Re moment at 1.5 K of 2.2(1) μ_B. The magnetic moment is consistent with $S = 3/2$ in K_2ReI_6 with three unpaired electrons on Re^{4+}. The Shubnikov magnetic space group of K_2ReI_6 is $P\bar{1}$. Any weak spin-canting causing a ferromagnetic component is too small to be observed within the current neutron data. Figure 7C shows the intensity of the magnetic peak as the temperature changing from 1.5 to 40 K. The intensity starts to grow around 24 K, matching the expected transition temperature.

DOI: 10.1021/acs.jpcc.8b11371
J. Phys. Chem. C 2019, 123, 1645−1652

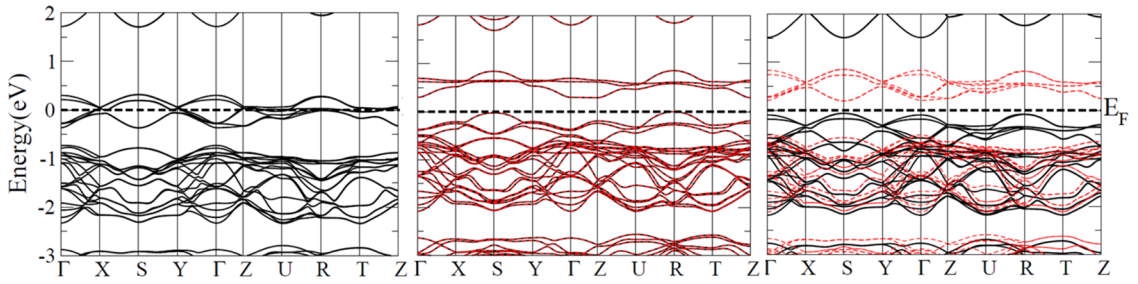

Figure 8. Calculated ab initio electronic band structures of nonmagnetic (NM), antiferromagnetic (AFM), and ferromagnetic (FM) models with spin−orbit coupling (SOC) included.

Spin-Canting in K_2ReI_6. We can estimate the canting angle (θ) through $\sin(\theta) = M_R/M_S$ solely contributed from the rotating of Re@I_6 octahedral cluster. M_R is the remnant magnetization determined by extrapolating the $M(H)$ data in the high field, which is 0.023 μ_B from Figure 6. M_S is the saturation moment, 2.2(1) μ_B from neutron powder diffraction. Accordingly, the canting angle is approximately 1.19°, which is consistent with the previously observed one (1.2°) and significantly larger than the canting angle caused by the anisotropy field.[55] Moreover, the spin-canting angle is different from any observed geometric ones. Consequently, the DM interaction contributes critically to the spin-canting in K_2ReI_6. Considering the origin of spin-canting, we would like to connect the spin-canting with the spin−orbit coupling effects rather than the symmetric factor, especially after carefully examining the inversion center in the crystal structure of K_2ReI_6.[37,38] WIEN2k calculations using both local density approximation (LDA) and local spin density approximation with the spin−orbit coupling (SOC) were applied to K_2ReI_6 shown in Figure 7. A Hubbard U = 2 eV was incorporated into the calculation. The electronic structure of nonmagnetic (NM) model shows that the bands across the Fermi level are hybridized among electrons from Re-d and K-s and I-p orbitals. After including the spin-polarization, the total energies of ferromagnetic (FM) and antiferromagnetic (AFM) models decrease significantly, which indicates that the antiferromagnetic model is favored thermodynamically (E_{tot} (AFM) = −3.515 eV/K_2ReI_6; E_{tot} (FM) = −3.118 eV/K_2ReI_6; E_{tot} (NM) = 0 eV/K_2ReI_6). A band gap with the width ∼1.0 eV in the NM model can be observed around the Fermi level in Figure 8. Moreover, the magnetic moments about 2.091 μ_B solely locate on Re atoms with the spin−orbit coupling employed. The calculation results confirm that the Re in K_2ReI_6 has an electron configuration $5d^3$, the interplay between the SOC and electron−electron correlations splits the degenerate gives Re^{4+} in K_2ReI_6 the spin angular momentum of S = 3/2.

Insulating K_2ReI_6. Similar with other halides, K_2ReI_6 is corrosive to metals including the puck used to perform the electric transport measurements. Instead, the UV−vis−NIR spectrum measurements (Figure 9) were conducted to show the insulating properties of K_2ReI_6. The UV−vis−NIR spectrum uses the visible light to excite valence electrons to empty orbitals.[56] The band gap can be calculated by measuring the relative change of reflectance of light as it passes through the K_2ReI_6. The band gap is ∼1.026 eV since the reflectance is the lowest at wavelength of 1206 nm. On the basis of the theoretical band structure calculation, the antiferromagnetic insulating K_2ReI_6 contains the indirect band gap with the width ∼1.0 eV. The approximately experimental results match with the theoretical prediction with antiferromagnetic model very well.

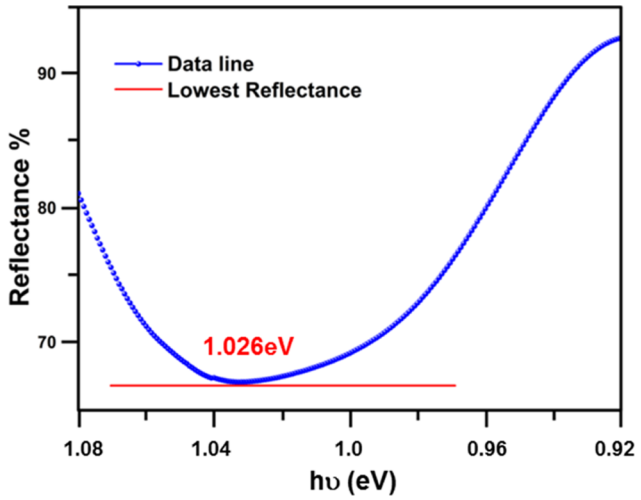

Figure 9. UV−vis−NIR spectrum measurement of K_2ReI_6. The blue line and dots and red line represent the reflectance data and the tangent line of the data line, which indicates the corresponding energy of the lowest reflectance.

CONCLUSIONS

Antiferromagnetic insulator, K_2ReI_6, was synthesized using solvent reactions, and its crystal structure and physical properties were thoroughly characterized. In K_2ReI_6, Re@I_6-distorted octahedral clusters with $5d^3$ electronic configuration are isolated from each other. Its magnetic properties show that it is an antiferromagnetic material with a weak ferromagnetic spin-canting at ∼24 K. The effective moments obtained from magnetic susceptibility and saturation moments refined from neutron diffraction confirm the S = 3/2 on Re^{4+}. The spin-canting angle is ∼1.19°, which indicates that the primary origin of spin-canting is from DM interactions rather than crystalline anisotropy. Optical measurements suggest that it is an insulator with a band gap of ∼1.0 eV. The theoretical results confirmed the magnetic moments solely from Re^{4+}, and band gap is around ∼1.0 eV. First-principles electronic structure calculations with SOC and spin-polarization substantiate the antiferromagnetic insulating properties. The K_2ReI_6 with isolated Re@I_6 octahedral cluster provides an ideal platform to study how the SOC influences the magnetic properties of $5d^3$ transition-metal halides.

DOI: 10.1021/acs.jpcc.8b11371
J. Phys. Chem. C 2019, 123, 1645−1652

■ ASSOCIATED CONTENT

Supporting Information

The Supporting Information is available free of charge on the ACS Publications website at DOI: 10.1021/acs.jpcc.8b11371.

Anisotropic thermal displacements; temperature-dependent magnetization measured at different applied fields (PDF)

Crystallographic anisotropic thermal displacements, magnetic data (CIF)

■ AUTHOR INFORMATION

Corresponding Author

*E-mail: weiweix@lsu.edu.

ORCID

Weiwei Xie: 0000-0002-5500-8195

Notes

The authors declare no competing financial interest.

■ ACKNOWLEDGMENTS

W.X. deeply appreciates constructive suggestions from reviewers to improve the paper and the thoughtful research discussion with Prof. David Mandrus (University of Tennessee, Knoxville), Prof. Jiaqiang Yan (Oak Ridge National Laboratory and University of Tennessee, Knoxville), and Dr Zhijun Wang (Institute of Physics, Chinese Academy of Science). X.G. and W.X. thank Dr Tai Kong, Danrui Ni, and Tia Lee (Princeton University) for UV−vis−NIR measurements. W.X. also thanks Prof. Robert Cava (Princeton University) for correcting the written English. The work at LSU is supported by the National Science Foundation under NSF-OIA-1832967. This research used resources at the High Flux Isotope Reactor, a DOE Office of Science User Facility operated by the Oak Ridge National Laboratory.

■ REFERENCES

(1) Balents, L. Spin liquids in frustrated magnets. *Nature* **2010**, *464*, 199.

(2) Lee, P. A. Quantum spin liquid: a tale of emergence from frustration. *J. Phys.: Conf. Ser.* **2014**, *529*, No. 012001.

(3) Zhou, Y.; Kanoda, K.; Ng, T. K. Quantum spin liquid states. *Rev. Mod. Phys.* **2017**, *89*, No. 025003.

(4) Savary, L.; Balents, L. Quantum spin liquids: a review. *Rep. Prog. Phys.* **2016**, *80*, No. 016502.

(5) Banerjee, A.; Bridges, C. A.; Yan, J. Q.; Aczel, A. A.; Li, L.; Stone, M. B.; Granroth, G. E.; Lumsden, M. D.; Yiu, Y.; Knolle, J.; Bhattacharjee, S.; et al. Proximate Kitaev quantum spin liquid behaviour in a honeycomb magnet. *Nat. Mater.* **2016**, *15*, 733.

(6) Kim, B. J.; Ohsumi, H.; Komesu, T.; Sakai, S.; Morita, T.; Takagi, H.; Arima, T. H. Phase-sensitive observation of a spin-orbital Mott state in Sr_2IrO_4. *Science* **2009**, *323*, 1329−1332.

(7) Weng, H.; Fang, C.; Fang, Z.; Bernevig, B. A.; Dai, X. Weyl Semimetal Phase in Noncentrosymmetric Transition-Metal Monophosphides. *Phys. Rev. X* **2015**, *5*, No. 011029.

(8) Plumb, K. W.; Clancy, J. P.; Sandilands, L. J.; Shankar, V. V.; Hu, Y. F.; Burch, K. S.; Kee, H. Y.; Kim, Y. J. α-$RuCl_3$: A spin-orbit assisted Mott insulator on a honeycomb lattice. *Phys. Rev. B* **2014**, *90*, No. 041112.

(9) Moore, J. E. The birth of topological insulators. *Nature* **2010**, *464*, 194.

(10) Burkov, A. A.; Balents, L. Weyl Semimetal in a Topological Insulator Multilayer. *Phys. Rev. Lett.* **2011**, *107*, No. 127205.

(11) Xu, S. Y.; Belopolski, I.; Alidoust, N.; Neupane, M.; Bian, G.; Zhang, C.; Sankar, R.; Chang, G.; Yuan, Z.; Lee, C. C.; Huang, S. M.; Zheng, H.; Ma, J.; Sanchez, D. S.; Wang, B. K.; Bansil, A.; Chou, F.; Shibayev, P. P.; Lin, H.; Jia, S.; Hasan, M. Z. Discovery of a Weyl fermion semimetal and topological Fermi arcs. *Science* **2015**, *349*, 613−617.

(12) Lv, B. Q.; Weng, H. M.; Fu, B. B.; Wang, X. P.; Miao, H.; Ma, J.; Richard, P.; Huang, X. C.; Zhao, L. X.; Chen, G. F.; Fang, Z.; Dai, X.; Qian, T.; Ding, H. Experimental discovery of Weyl semimetal TaAs. *Phys. Rev. X* **2015**, *5*, No. 031013.

(13) Essin, A. M.; Moore, J. E.; Vanderbilt, D. Magnetoelectric Polarizability and Axion Electrodynamics in Crystalline Insulators. *Phys. Rev. Lett.* **2009**, *102*, No. 146805.

(14) Li, R.; Wang, J.; Qi, X.-L.; Zhang, S.-C. Dynamical axion field in topological magnetic insulators. *Nat. Phys.* **2010**, *6*, 284−288.

(15) Wan, X.; Turner, A. M.; Vishwanath, A.; Savrasov, S. Y. Topological semimetal and Fermi-arc surface states in the electronic structure of pyrochlore iridates. *Phys. Rev. B* **2011**, *83*, No. 205101.

(16) Awschalom, D. D.; Bassett, L. C.; Dzurak, A. S.; Hu, E. L.; Petta, J. R. Quantum Spintronics: Engineering and Manipulating Atom-Like Spins in Semiconductors. *Science* **2013**, *339*, 1174−1179.

(17) Bogani, L.; Wernsdorfer, W. Molecular spintronics using single-molecule magnets. *Nat. Mater.* **2008**, *7*, 179−186.

(18) Ladd, T. D.; Jelezko, F.; Laflamme, R.; Nakamura, Y.; Monroe, C.; O'Brien, J. L. Quantum computers. *Nature* **2010**, *464*, 45−53.

(19) Kroutvar, M.; Ducommun, Y.; Heiss, D.; Bichler, M.; Schuh, D.; Abstreiter, G.; Finley, J. J. Optically programmable electron spin memory using semiconductor quantum dots. *Nature* **2004**, *432*, 81−84.

(20) Knill, E. Quantum computing with realistically noisy devices. *Nature* **2005**, *434*, 39−44.

(21) Cao, H. B.; Banerjee, A.; Yan, J. Q.; Bridges, C. A.; Lumsden, M. D.; Mandrus, D. G.; Tennant, D. A.; Chakoumakos, B. C.; Nagler, S. E. Low-temperature crystal and magnetic structure of α-$RuCl_3$. *Phys. Rev. B* **2016**, *93*, No. 134423.

(22) Banerjee, A.; Yan, J.; Knolle, J.; Bridges, C. A.; Stone, M. B.; Lumsden, M. D.; Mandrus, D. G.; Tennant, D. A.; Moessner, R.; Nagler, S. E. Neutron scattering in the proximate quantum spin liquid α-$RuCl_3$. *Science* **2017**, *356*, 1055−1059.

(23) Xiong, J.; Yan, J.; Aczel, A. A.; Woodward, P. M. Type I antiferromagnetic order in Ba_2LuReO_6: Exploring the role of structural distortions in double perovskites containing $5d^2$ ions. *J. Solid State Chem.* **2018**, *258*, 762−767.

(24) Calder, S.; Vale, J. G.; Bogdanov, N. A.; Liu, X.; Donnerer, C.; Upton, M. H.; Casa, D.; Said, A. H.; Lumsden, M. D.; Zhao, Z.; Yan, J. Q.; Mandrus, D. G.; Nishimoto, S.; van den Brink, J.; Hill, J. P.; McMorrow, D. F.; Christianson, A. D. Spin-orbit-driven magnetic structure and excitation in the 5*d* pyrochlore $Cd_2Os_2O_7$. *Nat. Commun.* **2016**, *7*, No. 11651.

(25) Tian, W.; Svoboda, C.; Ochi, M.; Matsuda, M.; Cao, H. B.; Cheng, J. G.; Sales, B. C.; Mandrus, D. G.; Arita, R.; Trivedi, N.; Yan, J. Q. High antiferromagnetic transition temperature of the honeycomb compound $SrRu_2O_6$. *Phys. Rev. B* **2015**, *92*, No. 100404.

(26) Nishimoto, S.; Katukuri, V. M.; Yushankhai, V.; Stoll, H.; Rößler, U. K.; Hozoi, L.; Rousochatzakis, I.; Van Den Brink, J. Strongly frustrated triangular spin lattice emerging from triplet dimer formation in honeycomb Li_2IrO_3. *Nat. Commun.* **2016**, *7*, No. 10273.

(27) Kim, H.-S.; Vijay Shankar, V.; Catuneanu, A.; Kee, H.-Y. Kitaev magnetism in honeycomb $RuCl_3$ with intermediate spin-orbit coupling. *Phys. Rev. B* **2015**, *91*, No. 241110.

(28) Taylor, A. E.; Calder, S.; Morrow, R.; Feng, H. L.; Upton, M. H.; Lumsden, M. D.; Yamaura, K.; Woodward, P. M.; Christianson, A. D. Spin-Orbit Coupling Controlled $J = 3/2$ Electronic Ground State in $5d^3$ Oxides. *Phys. Rev. Lett.* **2017**, *118*, No. 207202.

(29) Pesin, D.; Balents, L. Mott physics and band topology in materials with strong spin−orbit interaction. *Nat. Phys.* **2010**, *6*, 376−381.

(30) Abeysinghe, D.; Huq, A.; Yeon, J.; Smith, M. D.; zur Loye, H.-C. In-Situ Neutron Diffraction Studies of the Flux Crystal Growth of the Reduced Molybdates $La_4Mo_2O_{11}$ and $Ce_4Mo_2O_{11}$: Revealing Unexpected Mixed-Valent Transient Intermediates and Determining

DOI: 10.1021/acs.jpcc.8b11371
J. Phys. Chem. C 2019, 123, 1645−1652

the Sequence of Events during Crystal Growth. *Chem. Mater.* **2018**, *30*, 1187−1197.
(31) Laguna-Marco, M. A.; Kayser, P.; Alonso, J. A.; Martínez-Lope, M. J.; van Veenendaal, M.; Choi, Y.; Haskel, D. Electronic structure, local magnetism, and spin-orbit effects of Ir (IV)-, Ir (V)-, and Ir (VI)-based compounds. *Phys. Rev. B* **2015**, *91*, No. 214433.
(32) Shi, Y.; Guo, Y.; Yu, S.; Arai, M.; Sato, A.; Belik, A. A.; Yamaura, K.; Takayama-Muromachi, E. Crystal Growth and Structure and Magnetic Properties of the 5*d* Oxide Ca_3LiOsO_6: Extended Superexchange Magnetic Interaction in Oxide. *J. Am. Chem. Soc.* **2010**, *132*, 8474−8483.
(33) Rodriguez, E. E.; Poineau, F.; Llobet, A.; Kennedy, B. J.; Avdeev, M.; Thorogood, G. J.; Carter, M. L.; Seshadri, R.; Singh, D. J.; Cheetham, A. K. High Temperature Magnetic Ordering in the 4*d* Perovskite $SrTcO_3$. *Phys. Rev. Lett.* **2011**, *106*, No. 067201.
(34) Ovsyannikov, S. V.; Bykov, M.; Bykova, E.; Kozlenko, D. P.; Tsirlin, A. A.; Karkin, A. E.; Shchennikov, V. V.; Kichanov, S. E.; Gou, H.; Abakumov, A. M.; Egoavil, R.; et al. Charge-ordering transition in iron oxide Fe_4O_5 involving competing dimer and trimer formation. *Nat. Chem.* **2016**, *8*, 501.
(35) Kuroda, K.; Tomita, T.; Suzuki, M. T.; Bareille, C.; Nugroho, A. A.; Goswami, P.; Ochi, M.; Ikhlas, M.; Nakayama, M.; Akebi, S.; Noguchi, R.; et al. Evidence for magnetic Weyl fermions in a correlated metal. *Nat. Mater.* **2017**, *16*, 1090.
(36) Ren, Y.; Palstra, T. T. M.; Khomskii, D. I.; Pellegrin, E.; Nugroho, A. A.; Menovsky, A. A.; Sawatzky, G. A. Temperature-induced magnetization reversal in a YVO_3 single crystal. *Nature* **1998**, *396*, 441.
(37) Dzyaloshinsky, I. A thermodynamic theory of "weak" ferromagnetism of antiferromagnetics. *J. Phys. Chem. Solids* **1958**, *4*, 241−255.
(38) Moriya, T. Anisotropic superexchange interaction and weak ferromagnetism. *Phys. Rev.* **1960**, *120*, 91.
(39) González, R.; Chiozzone, R.; Kremer, C.; De Munno, G.; Nicolò, F.; Lloret, F.; Julve, M.; Faus, J. Magnetic Studies on Hexaiodorhenate (IV) Salts of Univalent Cations. Spin Canting and Magnetic Ordering in $K_2[ReI_6]$ with T_c = 24 K. *Inorg. Chem.* **2003**, *42*, 2512−2518.
(40) Morrow, J. C. X-Ray Powder Pattern and Unit Cell Dimensions of K_2ReI_6. *J. Phys. Chem.* **1956**, *60*, 19−20.
(41) Le Bail, A.; Duroy, H.; Fourquet, J. L. Ab-Initio Structure Determination of $LiSbWO_6$ by X-Ray Powder Diffraction. *Mater. Res. Bull.* **1988**, *23*, 447−452.
(42) Bruker. *Smart*; Bruker AXS Inc.: Madison, WI, 2012. https://www.bruker.com/products/x-ray-diffraction-and-elemental-analysis/single-crystal-x-ray-diffraction/sc-xrd-software/overview/sc-xrd-software/apex3.html.
(43) Sheldrick, G. M. Crystal structure refinement with SHELXL. *Acta Crystallogr., Sect. C: Struct. Chem.* **2015**, *71*, 3−8.
(44) Rodríguez-Carvajal, J. Recent advances in magnetic structure determination by neutron powder diffraction. *Phys. B* **1993**, *192*, 55−69.
(45) Wills, A. S. A new protocol for the determination of magnetic structures using Simulated Annealing and Representational Analysis-SARAh. *Phys. B* **2000**, *276−278*, 680−681.
(46) Wills, A. S. Indexing magnetic structures and crystallographic distortions from powder diffraction: Brillouin zone indexing. *Z Kristallogr. Suppl.* **2009**, *2009*, 39−44.
(47) Yusuf, S. M.; Rao, L. M. The magnetic domain effect in the local canted spin ferrite $Zn_{0.5}Co_{0.5}Fe_{2-x}Cr_xO_4$: A macroscopic and mesoscopic study. *J. Phys.: Condens. Matter* **1995**, *7*, 5891.
(48) Figgis, B. N.; Lewis, J. The Magnetochemistry of Complex Compounds. In *Modern Coordination Chemistry*; Lewis, J., Wilkins, R. G., Eds.; Wiley: New York, 1960; p 406.
(49) Landé, A. Über den anomalen Zeemaneffekt (Teil I). *Z. Phys.* **1921**, *5*, 231−241.
(50) Miessler, G. L.; Tarr, D. A. *Inorganic Chemistry*; Prentice-Hall, 1999; pp 358−360.
(51) Figgis, B. N.; Lewis, J.; Mabbs, F. E. The magnetic properties of some d^3-complexes. *J. Chem. Soc.* **1961**, 3138−3145.
(52) Kotani, M. On the Magnetic Moment of Complex Ions. (I). *J. Phys. Soc. Jpn.* **1949**, *4*, 293−297.
(53) Lu, H.; Chamorro, J. R.; Wan, C.; McQueen, T. M. Universal Single-Ion Physics in Spin−Orbit-Coupled d^5 and d^4 Ions. *Inorg. Chem.* **2018**, *57*, 14443−14449.
(54) Phelan, B. F.; Krizan, J.; Xie, W.; Gibson, Q.; Cava, R. J. New material for probing spin-orbit coupling in iridates. *Phys. Rev. B: Condens. Matter Mater. Phys.* **2015**, *91*, No. 155117.
(55) Wang, X. Y.; Wang, L.; Wang, Z. M.; Su, G.; Gao, S. Coexistence of spin-canting, metamagnetism, and spin-flop in a (4, 4) layered manganese azide polymer. *Chem. Mater.* **2005**, *17*, 6369−6380.
(56) Skoog, D. A.; Holler, F. J.; Crouch, S. R. *Principles of Instrumental Analysis*, 6th ed.; Thomson Brooks/Cole: Belmont, CA, 2007; pp 169−173.

DOI: 10.1021/acs.jpcc.8b11371
J. Phys. Chem. C 2019, 123, 1645−1652